A Mn(II) Coordination Polymer with Sulfate and *trans*-1,2-Bis(4-pyridyl)ethylene Bridges: Synthesis, Structure, Magnetic and Ferroelectric Properties

Wei Xu and Jian-Li Lin

Center of Applied Solid State Chemistry Research, Ningbo University, Ningbo, 315211, P. R. China

Reprint requests to Prof. Dr. Wei Xu. Fax: Int. +574/87600792. E-mail: yqzhengmc@163.com

Z. Naturforsch. **2013**, *68b*, 877 – 884 / DOI: 10.5560/ZNB.2013-3119
Received April 19, 2013

Reaction of $MnSO_4$ and *trans*-1,2-bis(4-pyridyl)ethene (bpe) results in a new coordination polymer, $[Mn(H_2O)_2(bpe)(SO_4)]\cdot H_2O$. The title complex crystallizes in the polar monoclinic space group *C*2. The octahedrally coordinated Mn atoms are bridged by sulfate anions and bpe ligands to form two-dimensional sheets with $(4^2\cdot6^3\cdot8)$ topology. This polar complex displays ferroelectricity with a remanent polarization ($2P_r$) of *ca.* 0.5779 $\mu C\,cm^{-2}$, a coercive field ($2E_c$) of 8.8 $kV\,cm^{-1}$, and a saturation of the spontaneous polarization (P_S) of *ca.* 0.4177 $\mu C\,cm^{-2}$. The magnetic behavior of the title complex suggests significant antiferromagnetic coupling interactions between Mn(II) ions bridged by sulfate anions. Furthermore, the title complex was subjected to elemental analysis, IR spectroscopic measurement and thermal analysis.

Key words: Manganese, *trans*-1,2-Bis(4-pyridyl)ethene, Sulfate, Coordination Polymer, Topology, Properties

Introduction

Metal-organic frameworks (MOFs) have been actively investigated because of not only their intriguing topological variety but also their potential applications in fields such as gas storage, separation, optics, and catalysis [1 – 3]. The structural types are totally dependent on metal ions with various coordination abilities, organic spacers with different binding sites, lengths, and directions. In this regard, organic linkers with *N*- or *O*-donor atoms have been often explored to produce a great number of MOFs with interesting structures and properties [4 – 6]. Among them, one of the most successful approaches has exploited bi-functional ligands such as 4,4'-bipyridine (bpy) and *trans*-1,2-bis(4-pyridyl)ethene (bpe) as linkers for the construction of solid phases with diverse topologies [7 – 10]. These bidentate organic ligands usually act as rigid joints linking the metal sites into polymeric cationic chains. Such chain structures can be further elaborated to form two- and/or three-dimensional polymers through other connections. The doubly charged sulfate anion may act not only as a charge-compensating and space-filling agent, but also as a ligand to metal sites which can effectively participate in the interconnection of such chains giving rise to unusual structural types [11 – 13]. In recent years, some examples of polymeric species containing both SO_4^{2-} anions and bpe ligands have been reported, including one-dimensional, two-dimensional and three-dimensional structures [14 – 16]. We are currently searching for novel coordination polymers based on bi-functional *N*-containing ligands [17, 18]. In the present contribution, we report the synthesis and characterization of a new mixed sulfate- and *trans*-1,2-bis(4-pyridyl)ethane-bridged Mn(II) polymer, $Mn(H_2O)_2(bpe)(SO_4)]\cdot H_2O$.

Results and Discussion

Description of the crystal structure

The asymmetric unit of the title complex consists of one Mn(II) cation, one bpe ligand, one sulfate anion, two aqua ligands and one water molecule (Fig. 1). The Mn atoms are octahedrally coordinated by two N atoms from bridging bpe ligands occupying the axial

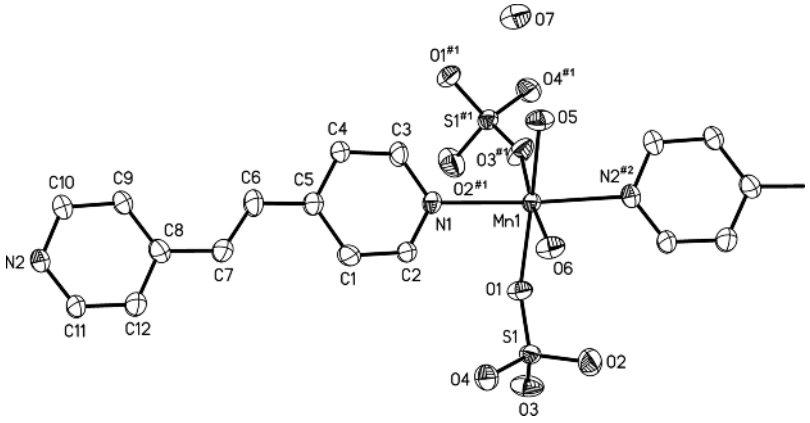

Fig. 1. ORTEP view of the structure of the title complex (45 % probability displacement ellipsoids). Symmetry transformations used to generate equivalent atoms: #1 = $-x+3/2$, $y+1/2$, $-z+2$; #2 = $x-1/2$, $y-1/2$, z.

positions, two O atoms from two bridging sulfate anions and two O atoms from water molecules occupying the equatorial sites. The Mn–O bond lengths vary from 2.132(5) to 2.232(5) Å, and the two Mn–N bond distances are 2.274(5) and 2.291(4) Å. The *trans* and *cisoid* bond angles fall in the regions 83.4(2) – 96.9(2)° and 170.3(2) – 176.2(2)° (Table 1), respectively, exhibiting considerable deviation from the ideal values (90°, 180°) for a regular octahedron, which indicates that the coordination polyhedron of the Mn(II) ions is slightly distorted. The bpe molecule exhibits the *trans*-conformation, and it acts as a bis-monodentate ligand connecting the Mn(II) ions to form -bpe-Mn-bpe- chains. Bond lengths and angles of the neutral bpe ligand agree well with those reported [19]. Each SO_4^{2-} anion provides two O atoms to bridge these chains to form sheets parallel to (001) (Fig. 2). The bipyridyl-bridged Mn(II) chains cross each other through sulfate zigzag bridging. The Mn···Mn separation is 5.988(2) Å through the sulfate ligands, and 13.911(2) Å through the bpe ligands. The Mn atoms can be treated as four-connected nodes, and the sulfate ligands and bpe ligands regarded as twofold connectors. As a result, the sheet $[Mn(H_2O)_2(bpe)(SO_4)]_n$ represents a $(4^2{\cdot}6^3{\cdot}8)$ topology of Sra type. The water molecules and SO_4^{2-} anions link the adjacent sheets through O–H···O hydrogen bond interactions to form a three-dimensional supramolecular network (Fig. 3). The O···O distances are in the range from 2.795(7) to 2.929(8) Å.

Thermal analysis

As shown in Fig. 4, the DTA curve of the title complex exhibits five endothermic peaks at 72, 117, 252, 368, and 842 °C and one exothermic peak at 515 °C. The TG curve shows that the title complex decomposes in three steps. The first step marks two continuous endothermic dehydrations with a weight loss of 15 % from room temperature to 150 °C corresponding to the calculated value of 14 % for two moles of aqua ligands and one water molecule. The weight loss of 48 % in the second step between 140 and 385 °C is in good agreement with the value of 47 % calculated for the loss of the bpe ligand. The intermediate may be "$MnSO_4$". Upon further heating, the weight of the brown residue remaining after heating above 850 °C is 18 %, close to the calculated value of 19 % for a mole of Mn_2O_3 (space group $Ia3$) which was identified by PXRD.

Magnetic properties

The temperature dependence of the magnetic susceptibility χ_m of the title complex was investigated in the range 2 – 300 K with an applied field of 1 kOe (Fig. 5). Upon cooling the sample, the χ_m value increases, reaching a maxium of 0.60 $cm^3\,K\,mol^{-1}$ at 2 K. The room-temperature value of $\chi_m T$ is 3.78 $cm^3\,K\,mol^{-1}$, smaller than the expected value (4.37 $cm^3 \cdot K \cdot mol^{-1}$) for one non-interacting Mn(II) center with $S = 5/2$. The $\chi_m T$ value decreases upon lowering the temperature to reach a value of 1.20 $cm^3\,K\,mol^{-1}$ at 2 K, indicating the occurrence of an antiferromagnetic interaction between the manganese(II) ions. The χ_m can be fit to the Curie-Weiss equation $\chi_m = C/(T-\Theta)$ with the Curie constant $C = 4.20(2)$ $cm^3\,K\,mol^{-1}$ and a Weiss constant

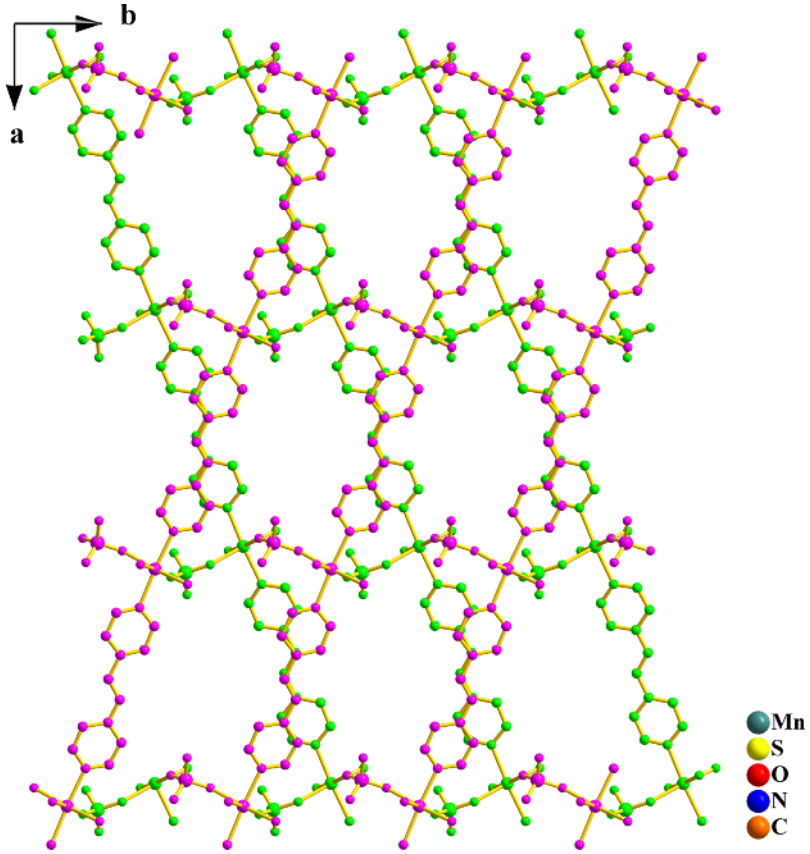

Fig. 2 (color online). View of the two-dimensional sheet formation of the title complex.

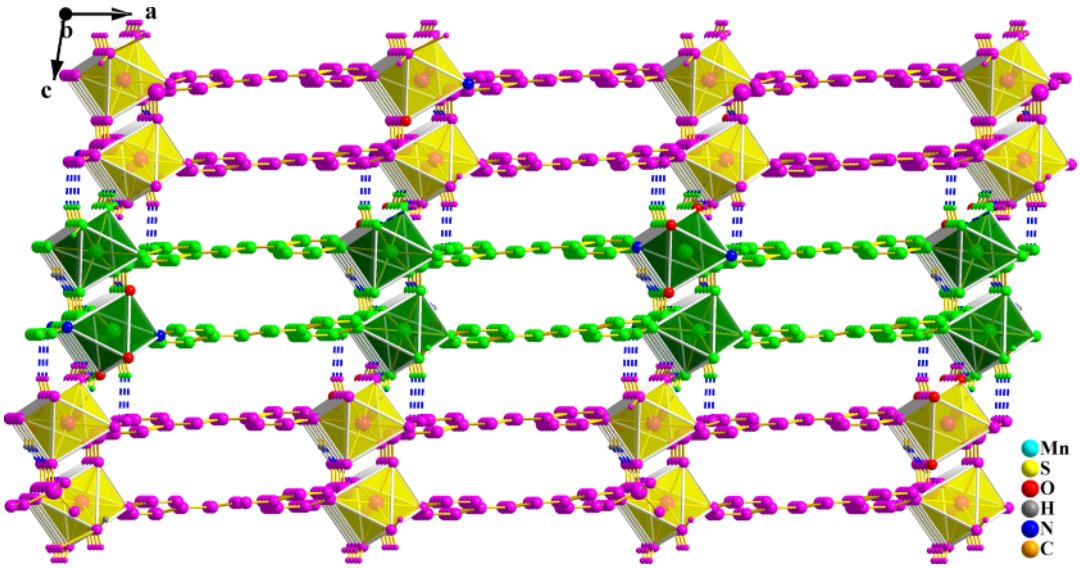

Fig. 3 (color online). Supramolecular assembly of the three-dimensional network generated *via* hydrogen bonds (dashed lines) in the title compound.

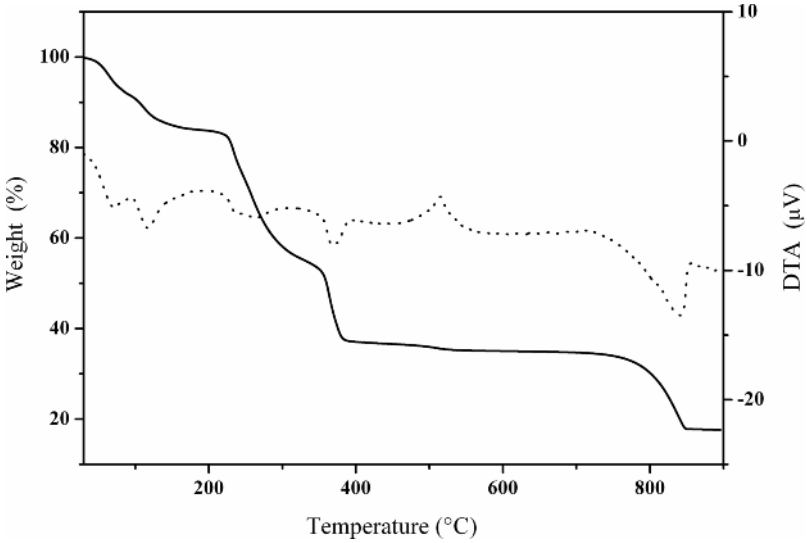

Fig. 4. TG-DTA curves for the title compound.

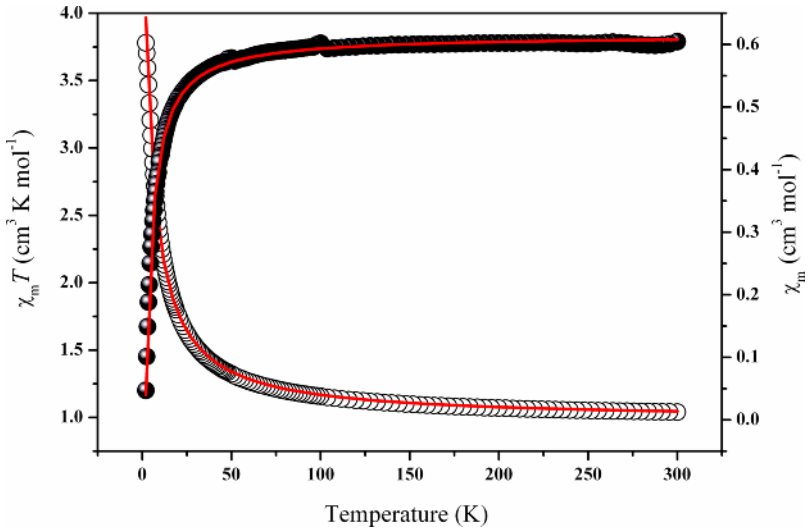

Fig. 5 (color online). Temperature dependence of the magnetic susceptibility of title complex. Solid lines represent the best fit.

of $\Theta = -4.54(6)$ K. The small negative Weiss constant also suggests weak antiferromagnetic interactions between the nearest neighbor Mn atoms. Since bpe is a long bridging dipyridinic ligand, which is only able to propagate very weak antiferromagnetic interactions between the metal centers, the magnetic coupling between the Mn(II) ions is probably achieved only through the bridging sulfate groups, giving a 1D magnetic ineraction. Owing to the very weak magnetic interactions between the ions, the expression in Eq. 1 is corrected using the molecular field approximation (Eq. 2), to which the present measured magnetic susceptibility data are fitted [20].

$$\chi = \frac{Ng^2\beta^2 S(S+1)}{3kT}\frac{1+u}{1-u} \qquad u = \coth\left[\frac{JS(S+1)}{kT}\right] - \left[\frac{kT}{JS(S+1)}\right] \tag{1}$$

$$\chi_m = \frac{\chi}{1-(2zJ'/Ng^2\beta^2)/\chi} \tag{2}$$

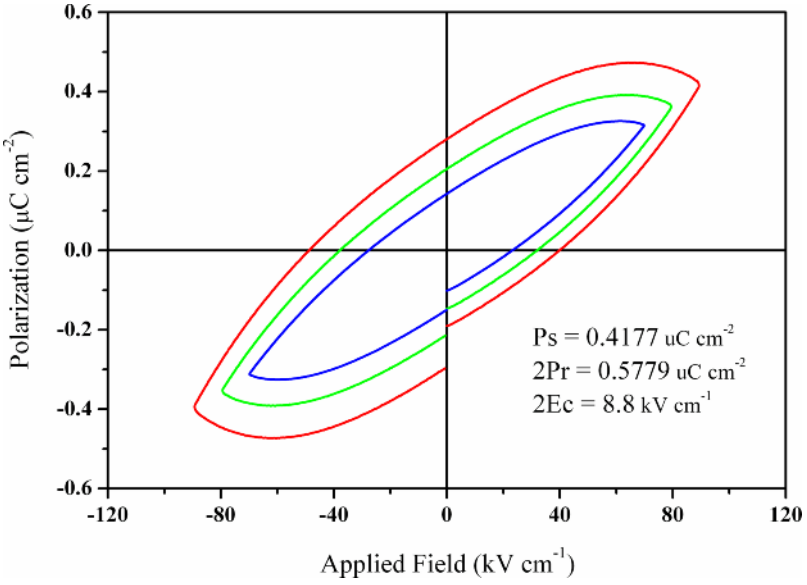

Fig. 6 (color online). Electric hysteresis loop for a powdered sample in the form of a pellet on a ferroelectric tester at room temperature.

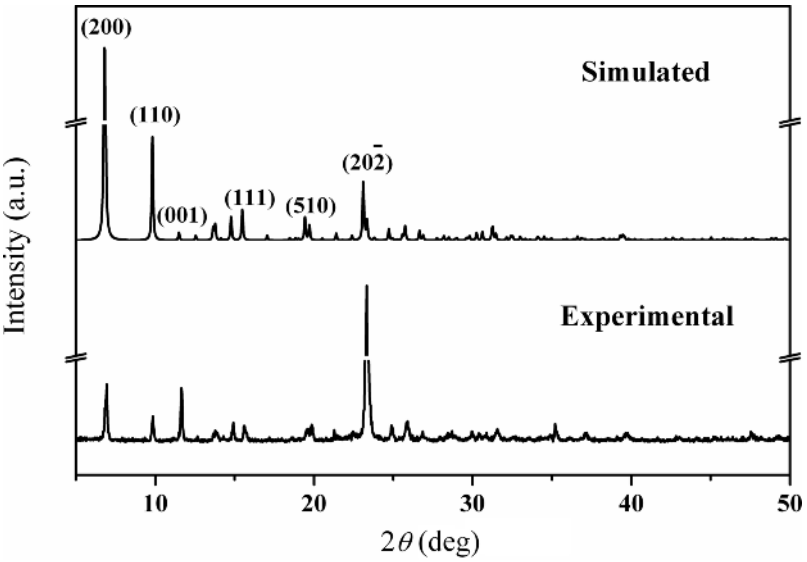

Fig. 7. Experimental and simulated PXRD pattern.

By using least-squares methods, a satisfactory fit of the data was gained with the set of parameters $J = -0.30(1)\,\mathrm{cm}^{-1}$, $zJ' = -0.01(1)\,\mathrm{cm}^{-1}$, and $g = 1.87$, and the agreement factor $R = \sum[(\chi_\mathrm{m})_\mathrm{obs} - (\chi_\mathrm{m})_\mathrm{calc}\,\mathrm{d}]^2/[(\chi_\mathrm{m})_\mathrm{obs}]^2$ is 2.8×10^{-4}, in which the negative J and zJ' values clearly indicate the existence of the dominant antiferromagnetic coupling between the adjacent Mn ions, consistent with the magnetic behavior illustrated by the $\chi_\mathrm{m}T$ *versus* T plot (Fig. 5).

Ferroelectric properties

It is well known that a non-centrosymmetric crystal structure is a prerequisite for many technologically im-

portant properties such as ferroelectricity and second-order nonlinear optical behavior [21]. The space group $C2$ (C_2^3) belongs to one of the 10 polar crystallographic point groups [1 (C_1), 2 (C_2), m (C_s), mm2 (C_{2v}), 3 (C_3), 3m (C_{3v}), 4 (C_4), 4mm (C_{4v}), 6 (C_6), 6mm (C_{6v}); Hermann-Mauguin notation, Schoenflies notation in parentheses], a prerequisite for ferroelectricity. Its ferroelectric properties were examined. Experimental results indicate that there exists an electric hysteresis loop that is a typical ferroelectric feature (Fig. 6). A remanent polarization $2P_r = 0.5779\ \mu C\,cm^{-2}$, a coercive field $2E_c = 8.8\ kV\,cm^{-1}$, and a saturation of the spontaneous polarization $P_s = 0.4177\ \mu C\,cm^{-2}$ have been determined. The P_s value is slightly higher than that of the typical ferroelectric compound Rochelle salt ($NaKC_4H_4O_6{\cdot}4H_2O$, $P_s = 0.25\ \mu C\,cm^{-2}$), but significantly smaller than that found in KH_2PO_4 (*ca.* $5\ \mu C\,cm^{-2}$).

Conclusion

In summary, we have synthesized a new two-dimensional sheet coordination polymer, $[Mn(H_2O)_2(bpe)(SO_4)]{\cdot}H_2O$, in which Mn(II) ions are interconnected by sulfate and *trans*-1,2-bis(4-pyridyl)ethene ligands into layers, corresponding to the Schläfli symbol $4^2 \cdot 6^3 \cdot 8$. The preliminary experimental results show that the title complex is a potential candidate for ferroelectricity. Using this synthetic approach will provide us with a potential route to prepare other novel coordination polymers with interesting structures, topologies and properties.

Experimental Section

Materials and physical methods

All chemicals of reagent grade were commercially available and used without further purification. The C, H, N and S microanalysis was performed with a Perkin Elmer 2400II CHNO/S elemental analyzer. The FT-IR spectrum was recorded from KBr pellets in the range $4000 - 400\ cm^{-1}$ on a Shimadzu FTIR-8900 spectrometer. Thermogravimetric measurement was carried out from r. t. to 900 °C on preweighed samples in an air stream using a Seiko Exstar 6000 TG/DTA 6300 apparatus with a heating rate of $10\ °C\,min^{-1}$. The temperature-dependent magnetic susceptibility was determined with a Quantum Design SQUID magnetometer (Quantum Design Model MPMS-7) in the temperature range 2 – 300 K with an applied field of 1 kOe (1 kOe = $7.96 \times 10^4\ A\,m^{-1}$). The ferroelectric property of the solid-state sample was measured on a pellet of a powdered sample

Table 1. Selected bond lengths (Å), angles (deg) and hydrogen bond parameters for **1** with estimated standard deviations in parentheses[a].

1			
Distances			
Mn1 – O1	2.182(4)	Mn1 – O6	2.176(4)
Mn1 – O3$^{\#1}$	2.132(5)	Mn1 – N1	2.291(4)
Mn1 – O5	2.232(5)	Mn1 – N2$^{\#2}$	2.274(5)
Angles			
O1 – Mn1 – O3$^{\#1}$	96.9(2)	O3$^{\#1}$–Mn1–N2$^{\#2}$	84.9(2)
O1 – Mn1 – O5	170.3(2)	O5 – Mn1 – O6	83.4(2)
O1 – Mn1 – O6	87.8(2)	O5 – Mn1 – N1	87.4(2)
O1 – Mn1 – N1	88.5(2)	O5 – Mn1 – N2$^{\#2}$	88.9(2)
O1 – Mn1 – N2$^{\#2}$	95.2(2)	O6 – Mn1 – N1	89.6(2)
O3$^{\#1}$–Mn1–O5	92.1(2)	O6 – Mn1 – N2$^{\#2}$	91.0(2)
O3$^{\#1}$–Mn1–O6	174.0(2)	N1 – Mn1 – N2$^{\#2}$	176.2(2)
O3$^{\#1}$–Mn1–N1	94.3(2)		

Hydrogen bond parameters (Å, deg)				
D–H···A	d(D–H)	d(H···A)	d(D–H···A)	∠(D–H···A)
O5–H5A···O4$^{\#3}$	0.81	2.03	2.811(7)	164
O5–H5B···O7	0.81	1.91	2.690(6)	164
O6–H6B···O2$^{\#3}$	0.82	1.90	2.730(7)	166
O6–H6C···O5$^{\#4}$	0.84	2.37	3.146(8)	154
O7–H7B···O2$^{\#5}$	0.84	1.99	2.795(7)	161
O7–H7C···O1$^{\#1}$	0.84	2.20	2.929(8)	145

[a] Symmetry transformations used to generate equivalent atoms: #1 = $-x+3/2$, $y+1/2$, $-z+2$; #2 = $x-1/2$, $y-1/2$, z; #3 = $-x+3/2$, $y+1/2$, $-z+1$; #4 = $-x+3/2$, $y-1/2$, $-z+1$; #5 = x, $y+1$, z.

Table 2. Crystal structure data for **1**.

	1
Formula	$C_{12}H_{16}MnN_2O_7S$
M_r	387.27
Crystal size, mm^3	$0.38 \times 0.15 \times 0.12$
Crystal system	monoclinic
Space group	$C2$ (no. 5)
a, Å	26.123(5)
b, Å	9.570(2)
c, Å	7.750(2)
β, deg	99.14(3)
V, Å^3	1912.7(7)
Z	4
$D_{calcd.}$, g cm^{-3}	1.3
$\mu(MoK_\alpha)$, mm^{-1}	0.8
$F(000)$	796
hkl range	$-33 \le h \le 33$ $-9 \le k \le 12$ $-9 \le l \le 10$
$((\sin\theta)/\lambda)_{max}$, Å^{-1}	0.65
Refl. measured / unique / R_{int}	3771 / 3052 / 0.078
Param. refined	208
$R(F)$ / $wR(F^2)$	0.0629 / 0.1751
GoF (F^2)	1.110
Flack parameter	0.00(4)
$\Delta\rho_{fin}$(max / min), e Å^{-3}	0.70 / −0.54

using a Premier station ferroelectric tester at room temperature while the sample was immersed in insulating oil.

Synthesis of [Mn(H$_2$O)$_2$(bpe)(SO$_4$)]·H$_2$O

Under stirring, 0.169 g (1 mmol) $MnSO_4 \cdot H_2O$ was dissolved in 30 mL $C_2H_5OH - H_2O$ mixed solvent ($v/v = 1:1$), then 0.182 g (1 mmol) *trans*-1,2-bis(4-pyridyl)ethene was added. The resulting mixture was stirred at 70 °C for 15 min and filtered, and the filtrate then allowed to stand at room temperature. Slow evaporation for one day afforded yellow block-shaped crystals (yield: 68 % based on the initial $MnSO_4$ input). The phase purity of the crystalline product was checked by comparing an experimental powder X-ray diffraction (PXRD) pattern with the one simulated on the basis of the single-crystal data (Fig. 7). The slight differences in intensities between the experimental and calculated spectrum may be due to a preferred orientation of the crystalites. – Anal. for $C_{12}H_{16}MnN_2O_7S$: calcd. C 37.22, H 4.13, N 7.23, S 8.28 (%); found C 37.43, H 4.31, N 7.14, S 8.16 (%). – IR (KBr pellet, cm^{-1}): ν = 3447m, 3053w, 2932w, 1607vs, 1558w, 1504m, 1427s, 1356w, 1304m, 1117vs, 1011s, 978m, 825s, 617s, 546s.

Crystal structure determination

Powder X-ray diffraction measurements were carried out with a Bruker D8 Focus X-ray diffractometer to check the phase purity. Single-crystal X-ray diffraction data were collected on a Rigaku R-Axis Rapid X-ray diffractometer operating with graphite-monochromatized MoK_α radiation (λ = 0.71073 Å). A suitable single crystal was selected under a polarizing microscope and fixed with epoxy cement on a fine glass fiber which was then mounted on the diffractometer for cell determination and subsequent data collection. The data are corrected for Lp and absorption effects. The programs SHELXS-97 and SHELXL-97 were used for structure solution and refinement, respectively [22 – 24]. The structure was solved by using Direct Methods, and all non-hydrogen atoms were located in subsequent difference Fourier syntheses. After several cycles of refinement, all hydrogen atoms associated with carbon atoms were geometrically generated, and the rest of the hydrogen atoms were located from successive Difference Fourier syntheses. Finally, all non-hydrogen atoms were refined with anisotropic displacement parameters by full-matrix least-squares techniques and hydrogen atoms with isotropic displacement parameters set to 1.2 or 1.5 times of the values for the associated heavier atoms. The crystal structure contains solvent-accessible voids of 217 Å^3, but showed no residual electron density in the voids. This might indicate that the crystal lost its solvent of crystallization without collapse of the structure. Detailed information about the crystal data and structure determination is summarized in Table 2.

CCDC 926061 contains the supplementary crystallographic data for this paper. These data can be obtained free of charge from The Cambridge Crystallographic Data Centre *via* www.ccdc.cam.ac.uk/data_request/cif.

Acknowledgement

This project was supported by the Open Foundation from Application of nonlinear Science and Technology in the Most Important Subject of Zhejiang (grant no. xkzl2006). Honest thanks are also extended to the K. C. Wong Magna Fund in Ningbo University.

[1] H. Furukawa, N. Ko, Y. B. Go, N. Aratani, S. B. Choi, E. Choi, A. Ö. Yazaydin, R. Q. Snurr, M. O'Keeffe, J. Kim, O. M. Yaghi, *Science* **2010**, *329*, 424–428.
[2] W. Zhang, R. G. Xiong, *Chem. Rev.* **2012**, *112*, 1163–1195.
[3] M. Kurmoo, *Chem. Soc. Rev.* **2009**, *38*, 1353–1379.
[4] D. J. Tranchemontagne, J. L. Mendoza-Cortés, M. O'Keeffe, J. Kim, O. M. Yaghi, *Chem. Soc. Rev.* **2009**, *38*, 1257–1283.

[5] J. J. Perry IV, P. L. Feng, S. T. Meek, K. Leong, F. P. Doty, M. D. Allendorf, *J. Mater. Chem.* **2012**, *22*, 10235–10248.
[6] D. Zhao, D. J. Timmons, D. Q. Yuan, H. C. Zhou, *Acc. Chem. Res.* **2010**, *44*, 123–133..
[7] K. Biradha, M. Sarkar, L. Rajput, *Chem. Commun.* **2006**, 4169–4179.
[8] S. Pramanik, C. Zheng, X. Zhang, T. J. Emge, J. Li, *J. Am. Chem. Soc.* **2011**, *133*, 4153–4155.
[9] Y. C. Ou, D. S. Zhi, W. T. Liu, Z. P. Ni, M. L. Tong, *Chem. Eur. J.* **2012**, *18*, 7357–7361.
[10] E. Sheepwash, V. Krampl, R. Scopelliti, O. Sereda, A. Neels, K. Severin, *Angew. Chem. Int. Ed.* **2011**, *50*, 3034–3037.
[11] J. H. Park, W. R. Lee, D. W. Ryu, K. S. Lim, E. A. Jeong, W. J. Phang, E. K. Koh, C. S. Hong, *Cryst. Growth Des.* **2012**, *12*, 2691–2698.
[12] Z. X. Wang, Q. F. Wu, H. J. Liu, M. Shao, H. P. Xiao, M. X. Li, *CrystEngComm* **2010**, *12*, 1139–1146.
[13] K. Y. Zou, J. L. Zhao, C. Liu, Z. Wang, Z. X. Li, *Eur. J. Inorg. Chem.* **2013**, 293–298.
[14] H. L. Hu, M. C. Suen, C. W. Yeh, J. D. Chen, *Polyhedron* **2005**, *24*, 1497–1502.
[15] D. Hagrman, R. P. Hammond, R. Haushalter, J. Zubieta, *Chem. Mater.* **1998**, *10*, 2091–2100.
[16] J. Y. Lee, S. J. Hong, C. Kim, Y. Kim, *Dalton Trans.* **2005**, 3716–3718.
[17] Y. Q. Zheng, W. Xu, H. L. Zhu, J. L. Lin, L. Zhao, Y. R. Dong, *CrystEngComm* **2011**, *13*, 2699–2708.
[18] W. Xu, Y. Q. Zheng, *J. Chem. Cryst.* **2012**, *42*, 313–317.
[19] A. M. P. Peedikakkal, J. J. Vittal, *Cryst. Growth Des.* **2011**, *11*, 4697–4703.
[20] F. Y. Li, L. Xu, G. G. Gao, *Dalton Trans.* **2007**, 1661–1664.
[21] W. Zhang, R. G. Xiong, *Chem. Rev.* **2012**, *112*, 1163–1195.
[22] G. M. Sheldrick, SHELXS/L-97, Programs for Crystal Structure Determination, University of Göttingen, Göttingen (Germany) **1997**.
[23] G. M. Sheldrick, *Acta Crystallogr.* **1990**, *A46*, 467–473.
[24] G. M. Sheldrick, *Acta Crystallogr.* **2008**, *A64*, 112–122.